Human Molecular Genetics, 2011, Vol. 20, No. 1 **51–63**
doi:10.1093/hmg/ddq431
Advance Access published on October 8, 2010

Drosophila FMRP regulates microtubule network formation and axonal transport of mitochondria

Aiyu Yao[1], Shan Jin[1,2], Xinhai Li[1], Zhihua Liu[1], Xuehua Ma[1], Jing Tang[1] and Yong Q. Zhang[1,*]

[1]Key Laboratory of Molecular and Developmental Biology, Institute of Genetics and Developmental Biology, Chinese Academy of Sciences, Beijing 100101, China and [2]College of Life Sciences, Hubei University, Wuhan, Hubei 430062, China

Received May 18, 2010; Revised and Accepted October 1, 2010

Fragile X syndrome, the most common form of inherited mental retardation, is caused by the absence of the fragile X mental retardation protein FMRP. The RNA-binding FMRP represses translation of the microtubule (MT)-associated protein 1B (MAP1B) during synaptogenesis in the brain of the neonatal mouse. However, the effect of FMRP on MTs remains unclear. Mounting evidence shows that the structure and the function of FMRP are well conserved across species from *Drosophila* to human. From a genetic screen, we identified *spastin* as a dominant suppressor of rough eye caused by *dfmr1* over-expression. *spastin* encodes an MT-severing protein, and its mutations cause neurodegenerative hereditary spastic paraplegia. Epistatic and biochemical analyses revealed that *dfmr1* acts upstream of or in parallel with *spastin* in multiple processes, including synapse development, locomotive behaviour and MT network formation. Immunostaining showed that both loss- and gain-of-function mutations of *dfmr1* result in an apparently altered MT network. Western analysis revealed that the levels of α-tubulin and acetylated MTs remained normal in *dfmr1* mutants, but increased significantly when *dfmr1* was over-expressed. To examine the consequence of the aberrant MTs in *dfmr1* mutants, we analysed the MT-dependent mitochondrial transport and found that the number of mitochondria and the flux of mitochondrial transport are negatively regulated by *dfmr1*. These results demonstrate that dFMRP plays a crucial role in controlling MT formation and mitochondrial transport. Thus, defective MTs and abnormal mitochondrial transport might account for, at least partially, the pathogenesis of fragile X mental retardation.

INTRODUCTION

Fragile X syndrome, the most common form of inherited mental retardation, is caused by the absence of the RNA-binding fragile X mental retardation protein FMRP. Although the *in vivo* functions of FMRP have been under intensive investigations in the last two decades, it remains unclear how the absence of FMRP leads to mental retardation (1–3). Multiple independent lines of evidence indicate that FMRP regulates microtubules (MTs). First, FMRP has been shown to bind and suppress the translation of MT-associated protein 1B (MAP1B) mRNA (4–6). MAP1B stabilizes MTs. In the neonatal mouse brain, FMRP suppresses the expression of MAP1B during synaptogenesis, and the elevated expression of MAP1B in *Fmr1* knockout mice leads to increased MT stability (7). Secondly, fractionation and western analysis showed that FMRP is associated with polymerized MTs (8,9). Thirdly, the *Drosophila* homologue of FMRP (dFMRP) suppresses the expression of Futsch, the fly homologue of MAP1B, in the nervous system (10,11). Together, these data establish an important role for FMRP in regulating MTs. However, evidence showing abnormal MTs associated with loss of FMRP *in vivo* has been scarce.

In addition to regulating MTs, FMRP has been shown to be an adaptor between FMRP-containing RNA granules and motor proteins. FMRP was found to be in the same protein complex with kinesin heavy chain in mouse brain homogenates (12). Specifically, FMRP interacts with the C-terminus of KIF3C, and disruption of the KIF3C function impedes the transport of FMRP-containing RNA granules in primary

*To whom correspondence should be addressed at: Key Laboratory of Molecular and Developmental Biology, Institute of Genetics and Developmental Biology, Chinese Academy of Sciences, Datun Road, Chao Yang District, Beijing 100101, China. Tel: +86 1064807611; Fax: +86 1064807611; Email: yqzhang@genetics.ac.cn

cultured neurons (8). More recently, Dictenberg *et al*. (13) reported that the C-terminal domain of FMRP interacts directly with kinesin light chain (KLC), the cargo-binding subunit of the KIF5 holoenzyme. In *Drosophila*, dFMRP associates with both kinesin heavy chain and dynein heavy chain, and knockdown of either of the two motors blocks the transport of dFMRP granules (14). These data together indicate a requirement of motor function for the transport of FMRP-positive cargos. However, a possible effect of FMRP on motor-mediated intracellular transport has not been closely examined.

From a genetic screen, we identified *spastin* as a dominant suppressor of the rough eye caused by *dfmr1* over-expression. *spastin* encodes an MT-severing protein, and mutations of *spastin* result in neurodegenerative hereditary spastic paraplegia (15–18). Epistatic and biochemical analyses revealed that *dfmr1* acts upstream of or in parallel with *spastin* in multiple processes, including neuromuscular synapse formation, locomotive control and MT network formation. Immunohistochemical analysis showed an apparently altered MT network in both loss- and gain-of-function *dfmr1* mutants. Moreover, the number of mitochondria and the flux of mitochondrial transport in axons are negatively regulated by *dfmr1*. Thus, *dfmr1* is required for both MT formation and mitochondrial transport, which offers novel insights into the pathogenesis of fragile X mental retardation.

RESULTS

spastin mutants or RNAi knockdown suppresses rough eye induced by *dfmr1* over-expression

To better understand the functions of dFMRP *in vivo*, we took advantage of the powerful genetics available in *Drosophila* to identify *dfmr1* interacting genes. Over-expression of *dfmr1* in the compound eye by the UAS-Gal4 system (19) led to a mild rough eye (compare Fig. 1A and B), consistent with earlier reports (10,20). Eye-specific over-expression of *dfmr1* was achieved by crossing *GMR-Gal4* with *EP3517* that carries a *UAS* element inserted in the 5' regulatory region of *dfmr1* (Fig. 1B). Modification of the rough eye indicates a putative *dfmr1* interacting gene. From the genetic screen, we found that *spastin*$^{5.75}$ nulls with the coding exons completely deleted (16) dominantly suppressed the rough eye caused by *dfmr1* over-expression (Fig. 1C; the effect of homozygous *spastin* null mutants on the *dfmr1* over-expression rough eye cannot be scored because they are adult lethal). *spastin* RNAi knockdown also suppressed the rough eye phenotype (Fig. 1D). Conversely, over-expression of *spastin* and *dfmr1* together enhanced the rough eye caused by over-expression of *dfmr1* or *spastin* alone (Table 1). To rule out any influence of the genetic background on the interaction between *dfmr1* and *spastin*, we examined the interaction in another independent system. Ectopic over-expression of *dfmr1* under the direct control of the *sevenless* enhancer also resulted in a rough eye phenotype [Fig. 1E and (20)]. Again, *spastin*$^{5.75}$ mutants dominantly and strongly suppressed the rough eye (compare Fig. 1E and F). Additionally, ubiquitous over-expression of *dfmr1* by *act-Gal4* was lethal, but *spastin* RNAi knockdown rescued the lethality (Table 1). It is worth pointing out that *spastin* RNAi knockdown showed a stronger effect in suppressing the lethality of ubiquitous *dfmr1* over-expression than heterozygous mutants (Table 1). This is

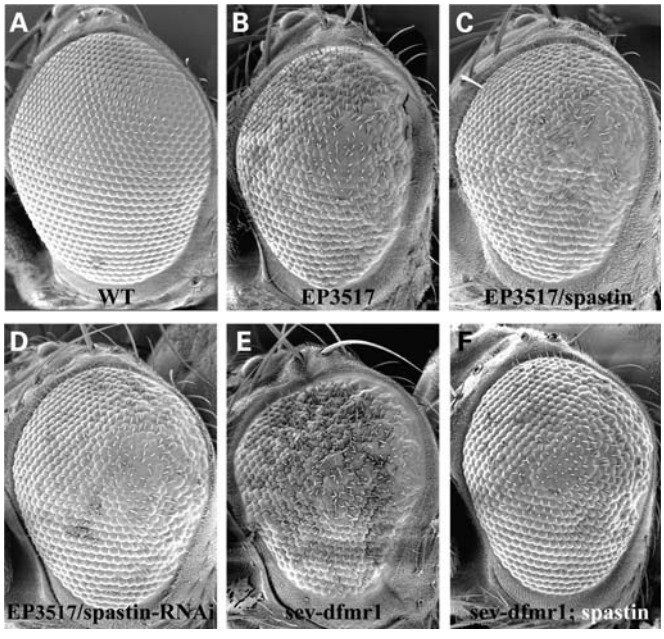

Figure 1. *spastin* mutants and RNAi knockdown suppress the rough eye phenotype induced by *dfmr1* over-expression. Scanning electron micrographs of adult eyes. (**A**) *GMR-Gal4/+* as the wild-type control (WT). (**B**) Over-expression of *dfmr1* by *GMR-Gal4* resulted in a mild rough eye phenotype (*GMR-Gal4/+*; *EP3517/+*). (**C** and **D**) Heterozygous *spastin* null mutant and RNAi knockdown suppressed the rough eye induced by *dfmr1* over-expression [(C) *GMR-Gal4/+*; *EP3517/spastin*$^{5.75}$ and (D) *GMR-Gal4/+*; *EP3517/spastin-RNAi*]. (**E**) *dfmr1* over-expression under the control of *sevenless* enhancer (*sev-dfmr1/+*) resulted in a rough eye. (**F**) *spastin* mutants dominantly suppressed the *sev-dfmr1* rough eye (*sev-dfmr1/+*; *spastin*$^{5.75}$*/+*).

Table 1. *spastin* mutants and RNAi knockdown suppress rough eye or lethality induced by *dfmr1* over-expression

Transgenes or alleles	*GMR-Gal4*	*GMR-Gal4, EP3517*	*sev-dfmr1*	*act-Gal4; EP3517*
spastin$^{5.75}$/+ (KZ)	na	S	S	N
spastin$^{17-7}$/+ (KZ)	na	S	S	N
spastin RNAi (KB)	N	S	na	S
UAS-spastin (KZ)	R	E	na	na
UAS-spastin (KB)	R	E	na	na

KZ and KB indicate stocks from K. Zinn (16) and K. Broadie (17), respectively. Over-expression of *dfmr1* or *spastin* by *GMR-Gal4* produced a rough eye. Co-over-expression of *spastin* and *dfmr1* enhanced the rough eye, whereas *spastin* RNAi knockdown or mutants suppressed the rough eye caused by over-expression of *dfmr1* driven by *GMR-Gal4* or under the control of the eye-specific *sevenless* promoter [*sev-dfmr1* (20)]. *spastin* RNAi knockdown also rescued the lethality caused by the ubiquitous over-expression of *dfmr1* driven by *act-Gal4*. E, enhance; N, no effect; na, not applicable or not assayed; R, rough eye; S, suppress.

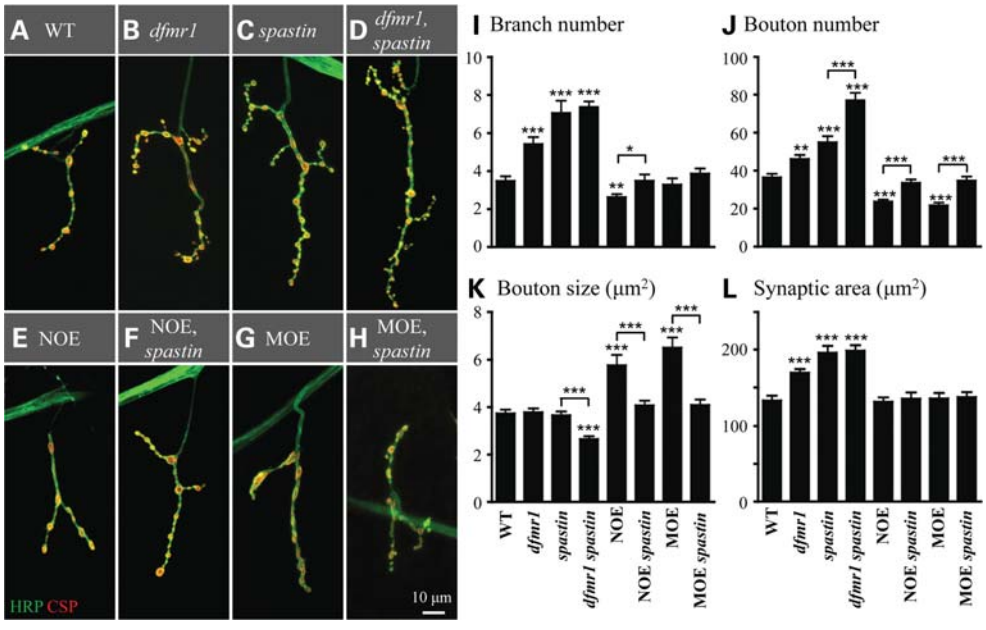

Figure 2. *dfmr1* and *spastin* convergently regulate synaptic growth on both pre- and post-synaptic side. Confocal images of NMJ4 synapses of abdominal segment A3 were labelled with anti-CSP in red and FITC-conjugated anti-HRP in green to reveal synaptic vesicle and neuronal membrane, respectively. Representative NMJ synapses of different genotypes are shown: (**A**) wild-type (WT); (**B**) $dfmr1^{50M}$; (**C**) $spastin^{5.75}$; (**D**) $dfmr1^{50M}$ $spastin^{5.75}$ double mutant; (**E**) pre-synaptic neuronal over-expression of *dfmr1* ($dfmr1^{NOE}$: *elav-Gal4*; *UAS-dfmr1*/+); (**F**) neuronal over-expression of dFMRP in the *spastin* homozygous null background (*elav-Gal4*; *UAS-dfmr1* $spastin^{5.75}$/$spastin^{5.75}$); (**G**) post-synaptic muscular over-expression of *dfmr1* ($dfmr1^{MOE}$: *C57-Gal4*/*UAS-dfmr1*) and (**H**) muscular over-expression of *dfmr1* in the *spastin* null background (*UAS-dfmr1* $spastin^{5.75}$/*C57-Gal4* $spastin^{5.75}$). The scale bar represents 10 μm. (**I**–**L**) Quantification of synaptic morphological features: branch number (I), bouton number (J), bouton size (K) and synaptic area (L). $n > 19$ for all genotypes assayed. Comparisons were made between each genotype with the wild-type control unless indicated otherwise. $^{*}P < 0.05$, $^{**}P < 0.01$, $^{***}P < 0.001$; error bars indicate SEM.

understandable as the RNAi knockdown probably decreases the expression of spastin by more than 50%. Taken together, the robust genetic interactions between *dfmr1* and *spastin* suggest that *spastin* is required for the pathogenesis caused by *dfmr1* over-expression.

dfmr1 and *spastin* convergently regulate synaptic growth on both pre- and post-synaptic side

Earlier work showed that *dfmr1* regulates synaptic growth negatively through repressing the expression of the MT-associated protein Futsch (10). Consistently, *dfmr1* mutants show an increased number of Futsch-positive cytoskeletal loops within synaptic boutons, further supporting a role of *dfmr1* in regulating MTs (21). *spastin* null mutants also show over-grown neuromuscular junction (NMJ) synapses (16), similar to that in *dfmr1* null mutants (10). We therefore examined the interaction between *dfmr1* and *spastin* at NMJ synapses to further understand how *dfmr1* and spastin regulate synaptic development.

We first confirmed that the NMJ synaptic terminals in *dfmr1* and *spastin* null mutants were overgrown as reported (Fig. 2) (10,16). To quantify this phenotype, we examined simple NMJ4 synapses that were double-labelled with the neuronal membrane marker anti-horseradish peroxidase (HRP) and the synaptic vesicle marker anti-cysteine string protein (CSP). Complete loss of *dfmr1* and *spastin* caused a significant increase in synaptic branching (5.43 ± 0.36 branches for *dfmr1*, 7.06 ± 0.64 for *spastin* and 3.48 ± 0.25 for wild-type; Fig. 2I), bouton number (46.10 ± 2.17 for *dfmr1*; 54.94 ± 3.14 for *spastin*, $P < 0.001$; 36.40 ± 1.87 for wild-type; Fig. 2J) and synaptic area (169.51 ± 4.83 μm^2 for *dfmr1*, 195.83 ± 9.15 μm^2 for *spastin* and 132.89 ± 6.25 μm^2 for wild-type; Fig. 2L). The synaptic overgrowth phenotype of *spastin* mutants was stronger than that of *dfmr1* mutants (compare Fig. 2C and B), although the average bouton size in the *spastin* and *dfmr1* mutants and the wild-type was all similar (Fig. 2K).

To determine the genetic interaction between *dfmr1* and *spastin*, we first generated and examined double mutants. The synaptic branch and the synaptic area of *dfmr1 spastin* double null mutants were comparable to those of *spastin* mutants ($P > 0.05$; Fig. 2I and L); however, there were more boutons (77.10 ± 3.91 for double mutants versus 54.94 ± 3.14 for *spastin* mutants; Fig. 2J) and smaller boutons (2.66 ± 0.12 μm^2 for double mutants versus 3.66 ± 0.16 μm^2 for *spastin* mutants; Fig. 2K) in the double mutants than there were in *spastin* and *dfmr1* single mutants, suggesting that *dfmr1* and *spastin* act in parallel to regulate synaptic growth. To further understand the interaction between *dfmr1* and *spastin*, we over-expressed dFMRP pre- or post-synaptically in a $spastin^{5.75}$ null background. Pre-synaptic over-expression of dFMRP driven by the pan-neuronal *elav-Gal4* (Fig. 2E) led to fewer (76% of wild-type) and larger (150% of wild-type) boutons than the wild-type, consistent with an earlier report (10). Remarkably, pre-synaptic over-expression of dFMRP ($dfmr1^{NOE}$) in the *spastin* null background completely rescued the bidirectional

NMJ phenotypes of the *dfmr1*^{NOE} and *spastin* mutants to the wild-type (3.50 ± 0.30 for branch number, 33.60 ± 1.6 for bouton number, 4.08 ± 0.19 μm^2 for bouton size and 135.37 ± 7.90 μm^2 for synaptic area; $P > 0.05$ for all four parameters compared with the wild-type; Fig. 2I–L). Post-synaptic over-expression of dFMRP also led to fewer (60% of wild-type) and larger boutons (173% of wild-type) than the wild-type. Interestingly, these synaptic defects were also restored to wild-type by homozygous *spastin*$^{5.75}$ null mutants (34.75 ± 2.26 for bouton number and 4.10 ± 0.23 μm^2 for bouton size; $P > 0.05$ for both parameters compared with wild-type; Fig. 2J and K). Together, these results demonstrate that *dfmr1* acts in parallel with *spastin* to inhibit synaptic growth.

spastin mutants rescue the locomotion impairment caused by muscular over-expression of *dfmr1*

Given that *dfmr1* and *spastin* interact in the eye development and NMJ synaptic growth (Figs 1 and 2), we sought to investigate whether both genes interact in controlling larval locomotive behaviour. We compared the coordinated behaviours of different animals using the larval roll-over assay, which involves turning a crawling larva to a totally inverted position and then recording the time the animal takes to fully right itself to the normal position. *dfmr1*^{50M} homozygous and hemizygous null mutants displayed faster roll-over than the wild-type (6.17 ± 0.56 s for homozygous mutant versus 14.7 ± 1.1 s for wild-type; Fig. 3). *spastin*$^{5.75}$ null mutants (6.82 ± 0.47 s), such as *dfmr1*^{50M} null mutants, rolled over more quickly than the wild-type. *dfmr1 spastin* double mutants showed a phenotype similar to that of the *dfmr1* or *spastin* single mutants. However, over-expression of *dfmr1* in muscles by *C57-Gal4* (*dfmr1*^{MOE}) strongly impaired the coordinated locomotion, with roll-over time increased to 227.6% (33.32 ± 2.95 s). The *dfmr1*^{MOE} animals stayed upside down for much longer and appeared to be struggling during a period of continuous, spastic muscle contractions that did not lead to the turning behaviour, whereas wild-type animals showed smooth, cooperative locomotion and turned over quickly. However, animals with *dfmr1* over-expression in the neural system induced by pan-neuronal *elav-Gal4* (*dfmr1*^{NOE}) rolled over normally, like the wild-type (13.05 ± 1.56 s for *dfmr1*^{NOE}). As a control, *C57-Gal4*, *elav-Gal4* and *UAS-dfmr1* transgenic flies alone without dFMRP over-expression showed normal locomotion (Fig. 3).

Remarkably, the locomotion impairment caused by muscular over-expression of *dfmr1* was fully rescued by heterozygous (17.0 ± 1.64 s for *dfmr1*^{MOE}, *spastin*/+; $P < 0.001$ compared with *dfmr1*^{MOE}, but $P > 0.05$ compared with the wild-type) and homozygous *spastin* null mutants (13.21 ± 1.18 s for *dfmr1*^{MOE}, *spastin*; $P < 0.001$ when compared with *dfmr1*^{MOE}, but $P > 0.05$ when compared with the wild-type; Fig. 3). Reciprocally, the faster roll-over of *spastin* homozygous mutants was rescued completely by over-expressing *dfmr1* in neural (14.22 ± 1.62 s) and muscular systems (13.21 ± 1.18 s). A possible explanation behind the reciprocal rescue of the locomotive defects is that *spastin* mutants may suppress the MT defects caused by *dfmr1* over-expression (discussed subsequently). Taken together, the similar locomotion defects of *dfmr1* and *spastin* mutants and the reciprocal rescuing effect of *dfmr1* over-expression in the *spastin* null background indicate that *dfmr1* and *spastin* work in parallel in regulating larval locomotion.

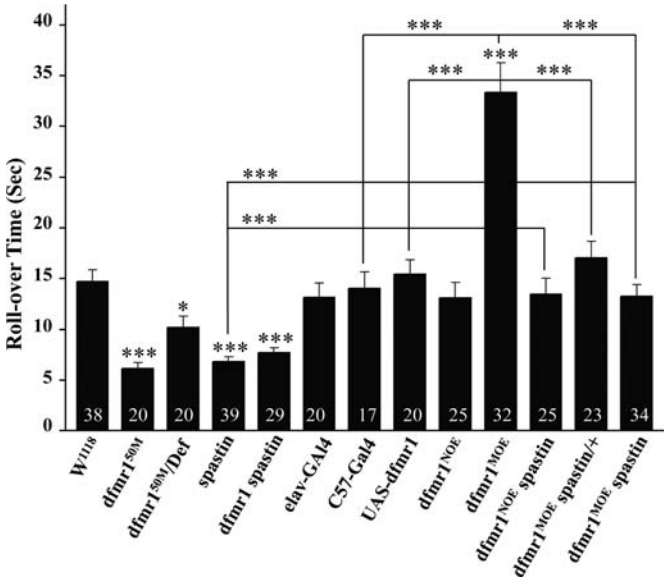

Figure 3. *spastin* mutants suppress the larval locomotive impairment caused by muscular over-expression of *dfmr1*. The roll-over assay was used to examine the larval locomotion ability of various genotypes. *dfmr1* and *spastin* mutants had significantly reduced roll-over times, whereas over-expression of *dfmr1* in muscles (*dfmr1*^{MOE}) but not in neurons (*dfmr1*^{NOE}) showed greatly impaired roll-over. However, heterozygous or homozygous *spastin*$^{5.75}$ null mutants completely rescued the compromised locomotion of *dfmr1*^{MOE} larvae. The number of animals tested for each genotype is indicated in each column. $^{*}P < 0.05$, $^{***}P < 0.001$; error bars indicate SEM.

dfmr1 regulates formation of the MT network

The above-mentioned genetic analysis showed that *dfmr1* acts in parallel with or upstream of *spastin*, which encodes an MT-severing protein. Additionally, *dfmr1* suppresses the expression of the MT-associated protein Futsch (10), but direct evidence demonstrating abnormal MTs in *dfmr1* mutants has so far been scarce. We therefore sought to determine whether *dfmr1* affects MTs. In the large multi-nucleated muscle cells from a wild-type third instar larva, a remarkable MT meshwork was revealed by anti-α-tubulin staining, with an obvious enrichment of MTs around the nucleus (Fig. 4A) (16,17,22). *dfmr1*^{50M} null mutants showed increased perinuclear MT density but reduced MT intensity in the central area among nuclei (Fig. 4B), whereas over-expression of *dfmr1* in muscles driven by *C57-Gal4* led to prominent thick parallel MT bundles with no enrichment of perinuclear MTs (Fig. 4C). The MT defects in *dfmr1* mutants were rescued to wild-type by a genomic transgene P[w^+: *dfmr1*] (Fig. 4D), demonstrating that the phenotypes are specifically caused by *dfmr1* mutations. To better define the MT defects, the intensity of α-tubulin staining in the perinuclear and central area was quantified (Fig. 4K–M). Compared with the wild-type, the intensity of the MT network in the perinuclear area was increased significantly in *dfmr1* mutants (200.22 ± 6.40 for

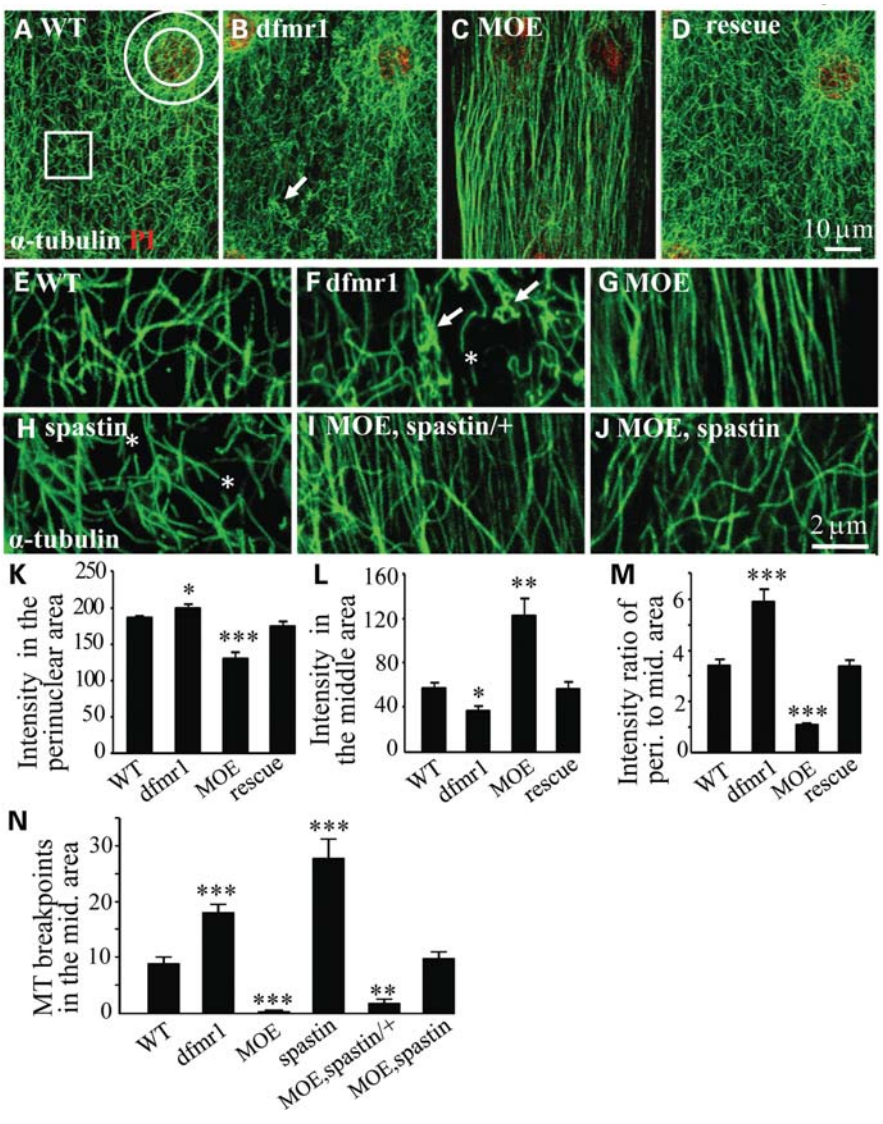

Figure 4. Altered expressions of *dfmr1* lead to disrupted MT network. (**A**–**D**) *Drosophila* larval muscles were stained with anti-α-tubulin to show the MT network (green) and with PI to show the nucleus (red) in WT (A), *dfmr1* null mutant ($dfmr1^{50M}$) (B), muscular over-expression (MOE) of *dfmr1* driven by *C57-Gal4* (C) and genomic rescue of *dfmr1* mutants P[w^+: *dfmr1*]; $dfmr1^{50M}$ (D). The scale bar represents 10 μm. The intensities of α-tubulin staining in the perinuclear [indicated by a concentric ring surrounding the nucleus in (A)] and in the central area among nuclei [indicated by a 10 × 10 μm square in (A)] were quantified. (**E**–**J**) The MT network in the central area at higher magnification for different genotypes. The arrows in (F) indicate MT tangles, and asterisks in (F) and (H) denote MT breakpoints. The scale bar in (J) represents 2 μm. (**K** and **L**) Statistical results of anti-α-tubulin staining intensities in the perinuclear (K) and central area (L) of different genotypes. (**M**) The ratio of the perinuclear α-tubulin staining intensity to that of the central area in different genotypes. (**N**) MT breakpoints in the middle area (20 × 20 μm) of muscle cells from different genotypes. Homozygous $spastin^{5.75}$ mutants and *dfmr1* over-expression in muscles driven by *C57-Gal4* reciprocally rescued the MT breakpoint defects to wild-type. $^{*}P < 0.05$, $^{**}P < 0.01$, $^{***}P < 0.001$; $n \geq 18$; error bars indicate SEM.

dfmr1 mutants versus 186.26 ± 2.33 for the wild-type), whereas the MT intensity in the central area was decreased significantly (37.04 ± 4.43 for *dfmr1* mutants versus 57.00 ± 6.04 for the wild-type) (Fig. 4K–M). In addition, the MT network was uneven and tangled in *dfmr1* mutants (Fig. 4B). Conversely, when *dfmr1* was over-expressed in muscles, the perinuclear MT intensity was decreased (129.53 ± 8.34 versus 186.26 ± 2.33), whereas the central area MT intensity was increased significantly (121.89 ± 15.56 for $dfmr1^{MOE}$ versus 57.00 ± 6.04 for the wild-type) (Fig. 4K–M). These results demonstrate that *dfmr1* regulates MT network formation.

Given the strong genetic interaction between *dfmr1* and *spastin* (Figs 1–3), and both dFMRP and spastin individually regulate MTs (Fig. 4A–D) (16–18,22,23), we therefore examined the interaction between *dfmr1* and *spastin* in controlling MT formation. The MT network in the middle area among nuclei of a muscle cell is better visualized at higher resolution (Fig. 4E–J). Compared with the evenly distributed MT network with smooth MT fibres in wild-type muscle cells (Fig. 4E), *dfmr1* mutants showed an unevenly distributed MT network with tangles and short MT fibres (Fig. 4F). Conversely, *dfmr1* over-expression resulted in thick parallel MT bundles (Fig. 4G). $spastin^{5.75}$ null mutants also exhibited

short MT fibres (Fig. 4H). Interestingly, *spastin* homozygous but not heterozygous null mutants fully rescued the thick parallel MT bundles in *dfmr1*^{MOE} cells to wild-type (Fig. 4I and J). Statistically, the MT breakpoints in the central area were increased significantly in *dfmr1* mutants (18.00 ± 1.37 per 400 μm^2 for *dfmr1*^{50M} mutants versus 8.66 ± 1.53 for the wild-type) as well as in *spastin*$^{5.75}$ null mutants (27.71 ± 3.35) (Fig. 4N). Conversely, when *dfmr1* was over-expressed in muscles (*dfmr1*^{MOE}), the number of MT breakpoints was significantly decreased (0.25 ± 0.16). The reduced MT breakpoints in *dfmr1* over-expressed animals were slightly rescued by heterozygous *spastin* mutation (1.90 ± 0.64), but completely rescued by homozygous *spastin* null mutation to wild-type (9.70 ± 1.36; $P > 0.05$) (Fig. 4N).

To determine the effect of the *dfmr1–spastin* interaction on MTs in neurons, we measured and compared the intensity of Futsch in the pre-synaptic terminals (Fig. 5). We found that the intensity of Futsch (the grey values of Futsch staining normalized to the Futsch-positive area reported by ImageJ) in *dfmr1* null mutants was significantly increased compared with wild-type (87.57 ± 4.88 for *dfmr1* mutants versus 73.88 ± 2.59 for wild-type, $P < 0.05$; Fig. 5F). Over-expression of *dfmr1* in pre-synaptic neurons driven by *elav-Gal4* led to a significantly decreased expression of Futsch (60.17 ± 1.87). The negative regulation of Futsch by dFMRP is consistent with previous findings (10,11,24). Similar to *dfmr1* mutants, *spastin* mutants also showed an increased level of Futsch (86.69 ± 4.88). Interestingly, *spastin* mutants fully rescued the reduced intensity of Futsch in *dfmr1*^{NOE} animals (74.39 ± 2.98 for *dfmr1*^{NOE}, *spastin* mutants; Fig. 5F). To eliminate the effect of the uneven distribution of Futsch in the synaptic terminals (anti-Futsch stains strongly at the proximal end but weakly at the distal end of synaptic terminals) among different genotypes, we calculated and compared the intensity of Futsch normalized to the synaptic area demarcated by anti-HRP staining between different genotypes (Supplementary Material, Fig. S1). Apparently, the Futsch intensities normalized to the HRP-demarcated synaptic area matched well with the Futsch intensities normalized to the Futsch-positive area in all the genotypes except in *spastin* mutants (compare Supplementary Material, Figs S1 and 5F). The *dfmr1–spastin* interaction in regulating Futsch intensity in pre-synaptic terminals recapitulates that in other systems (Figs 1–4).

To better understand the genetic interaction between *dfmr1* and *spastin*, we conducted biochemical assays. Co-immunoprecipitation with anti-dFMRP of muscle lysates showed that dFMRP and spastin are not present in the same complex (data not shown). Western analysis of larval muscles showed that the expression level of dFMRP (85 kDa) remains normal as the wild-type when *spastin* expression is altered (Fig. 6A), demonstrating that *spastin* does not affect the expression of *dfmr1*. However, the expression level of spastin (90 kDa) was significantly increased to 3.1 times of the wild-type ($P < 0.05$, $n = 4$) when *dfmr1* was over-expressed in muscles (*dfmr1*^{MOE}) driven by *C57-Gal4*, whereas loss of dFMRP did not affect the expression of spastin (Fig. 6B and C). The increased expression of spastin upon elevated expression of *dfmr1* supports the epistasis of *dfmr1* acting upstream of *spastin*, although the regulation mechanism is currently unknown.

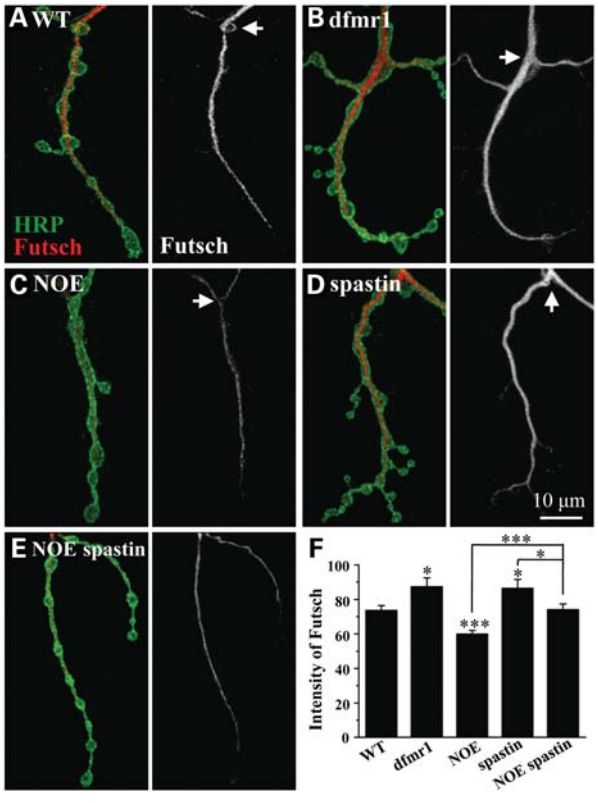

Figure 5. *spastin* mutants rescued the reduced level of Futsch at NMJ synapses of *dfmr1*^{NOE}. (**A–E**) Representative images of NMJ4 synapses in the abdominal segment A3 of third instar larvae co-stained with anti-Futsch to detect MTs (red) and anti-HRP to label pre-synaptic membrane (green) in WT (A), *dfmr1* null mutant (*dfmr1*^{50M}) (B), neuronal over-expression (NOE) of *dfmr1* driven by *elav-Gal4* (C), *spastin* null mutant (*spastin*$^{5.75}$) (D) and *dfmr1*^{NOE}, *spastin*$^{5.75}$[neuronal over-expression of *dfmr1* in homozygous *spastin* null background; (E)]. The arrows in (A)–(D) indicate the nerve innervation site. The scale bar in (D) represents 10 μm. (**F**) The intensity of Futsch staining normalized to the Futsch-positive area of the entire synaptic terminals starting from the innervation site was quantitatively analysed in different genotypes. $n \geq 11$; $^*P < 0.05$, $^{***}P < 0.001$; error bars indicate SEM.

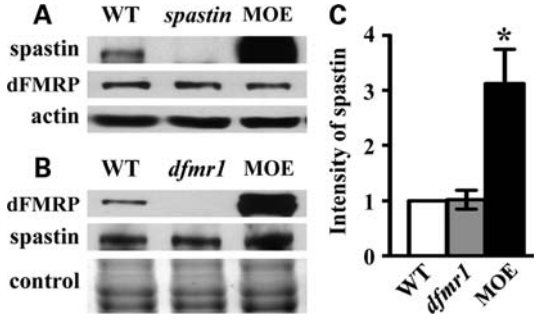

Figure 6. Elevated expression level of spastin when *dfmr1* is over-expressed. (**A**) The expression level of dFMRP is un-altered in loss- and gain-of-function mutants of *spastin*. Actin was used as loading control. MOE indicates muscular over-expression of spastin driven by *C57-Gal4*. (**B**) The expression level of spastin is significantly increased when *dfmr1* is over-expressed in muscles (MOE). The band sizes for dFMRP and spastin are 85 and 90 kDa, respectively. (**C**) Statistical analysis of spastin expression in loss- and gain-of-function mutants of *dfmr1*. $n = 4$; $^*P < 0.05$; error bars indicate SEM.

Total and acetylated α-tubulins are increased when *dfmr1* is over-expressed

To further understand the effect of *dfmr1* on MT, we examined the status of tubulins in different genotypes by fractionation followed by quantitative western analysis. Tubulins are present in two forms: soluble, unpolymerized tubulins and precipitable polymerized MTs. As shown in Figure 7, the total tubulins detected by an antibody against α-tubulin were increased significantly (by 46%) in animals with *dfmr1* over-expressed in muscles driven by *C57-Gal4* compared with the wild-type (Fig. 7A and C). The increased level of α-tubulin was observed in both soluble and precipitable fractions of *dfmr1* over-expressing animals (Fig. 7C), whereas *dfmr1* mutants showed normal levels of α-tubulins (Fig. 7C). To confirm the results, we determined the level of acetylated α-tubulins in the three genotypes. Acetylated α-tubulin is a marker for polymerized stable MTs (25). We found that the level of acetylated α-tubulins in *dfmr1* over-expressing animals was also significantly higher than that in the wild-type (1.6-fold greater than that of wild-type, Fig. 7B and D), concomitant with the increased level of α-tubulin. On the contrary, *spastin* null mutants showed reduced levels of acetylated α-tubulins (Fig. 7B and D). Interestingly, homozygous $spastin^{5.75}$ null mutants and $dfmr1^{MOE}$ animals reciprocally and completely rescued the altered expressions of acetylated α-tubulin to wild-type, whereas heterozygous *spastin* mutants had a weaker rescuing effect than the homozygous mutants (Fig. 7B and D). The level of total α-tubulin changed in accordance with that of acetylated α-tubulin in $dfmr1^{MOE}$ and $dfmr1^{MOE}$ *spastin* genotypes (data not shown). These results together further support the genetic interaction that *dfmr1* acts in parallel with *spastin*.

dfmr1 negatively regulates the number of mitochondria in axons and synaptic terminals

Given that *dfmr1* regulates MTs (Figs 4 and 7) and mitochondria transport is dependent on MTs (26), we sought to investigate whether MT-dependent transport of mitochondria was disrupted in *dfmr1* mutants. To this end, we first examined the axonal distribution of mitochondria labelled by a green fluorescent protein (GFP) tag (mito-GFP) in different genotypes. The mito-GFP was constructed by fusing the N-terminal 31 amino acids (a mitochondria-targeting sequence) from the human cytochrome *c* oxidase subunit VIII to the N-terminus of GFP (27). The expression of mito-GFP driven by the motor neuron-specific *D42-Gal4* labels mitochondria brightly in axons (Fig. 8A) (27–29). To our surprise, we found that the number of axonal mitochondria was inversely correlated to the expression levels of *dfmr1* (Fig. 8A–C). In $dfmr1^{50M}$ homozygous mutants, the number of mito-GFP-labelled mitochondria was increased significantly by 63.4% ($23.78 \pm 1.56/100\ \mu m^2$ for mutants versus $14.55 \pm 0.72/100\ \mu m^2$ for the wild-type; Fig. 8G). $dfmr1^{50M}/Df(3R)BSC621$ mutants also showed an increased number of mitochondria, similar to that in the homozygous mutants (data not shown), indicating that the increased number of mitochondria is caused specifically by *dfmr1* mutations. Conversely, neuronal over-expression of *dfmr1* led to a decrease in the number of mitochondria ($10.83 \pm 0.83/100\ \mu m^2$; Fig. 8G). Quantification of the area of mitochondria in axons showed trends similar to those of the number of mitochondria in different genotypes (compare Fig. 8H with G). As a control, the axonal distribution of synaptic vesicle precursors labelled by antibody staining against synaptotagmin (Syt) or CSP showed wild-type pattern in *dfmr1* mutants; similarly, the staining pattern for Bruchpilot, a synaptic active zone marker, was also normal when *dfmr1* was mutated or over-expressed (data not shown), indicating that *dfmr1* specifically affects the number of mitochondria but not other organelles in axons.

We further examined mitochondria at NMJ synapses to confirm the altered number of mitochondria in *dfmr1* mutants. As shown in Figure 8D, wild-type NMJ synapses contain GFP-labelled mitochondria as reported (29,30). However, the number of mitochondria was increased markedly in *dfmr1* mutants, but reduced when *dfmr1* was over-expressed by *D42-Gal4* (Fig. 8D–F). Due to the aggregation of mitochondria at the NMJ synapses of *dfmr1* mutants, which precluded quantification of the mitochondrial number (Fig. 8E), we quantified the area of GFP-tagged mitochondria at the NMJ terminals of the three different genotypes. Similar to that observed in axons (Fig. 8G and H), the percentage of mitochondrial area at NMJ synapses was increased significantly to 24.6% in *dfmr1* mutants, but decreased to 7.0% when *dfmr1* was over-expressed compared with 14.3% in the wild-type (Fig. 8I). The changes in the number of mitochondria in the soma of motor neurons were similar to those in axons and NMJ synapses when the expressions of *dfmr1* were altered (data not shown). The analysis of GFP-tagged mitochondria in both axons and NMJ synapses showed that the number of mitochondria is negatively regulated by *dfmr1*.

dFMRP affects flux and processivity of mitochondrial transport in axons

The results presented above showed disrupted MTs (Figs 4 and 7) and altered numbers of mitochondria in axons and NMJ synapses (Fig. 8). To examine a possible role for *dfmr1* in MT-based axonal transport of mitochondria, we conducted live imaging of motile mitochondria labelled with GFP in different genotypes. Mitochondrial transport displays salutatory bidirectional movement, in which moving mitochondria frequently start, stop and change direction (Supplementary Material, Movie S1), and we followed the commonly used parameters to describe mitochondrial transport (28). Flux is defined as the number of mitochondria moving into the bleached area per minute. Anterograde flux of mitochondria was significantly increased in *dfmr1* mutants (5.91 ± 0.11 for mutants versus 5.2 ± 0.22 for wild-type), but reduced when *dfmr1* was over-expressed compared with the wild-type (4.38 ± 0.25 for $dfmr1^{NOE}$) (Fig. 9D). Similarly, retrograde flux was increased significantly in *dfmr1* mutants (5.28 ± 0.19 for mutants versus 3.9 ± 0.10 for the wild-type), but was reduced in $dfmr1^{NOE}$ animals (2.27 ± 0.2; Fig. 9D; Supplementary Material, Movies S2 and S3). The bidirectional changes in the transport flux are positively correlated with alterations in the numbers of mitochondria observed in both loss- and gain-of-function *dfmr1* mutants (Fig. 8). Flux represents both the abundance of moving organelles and their

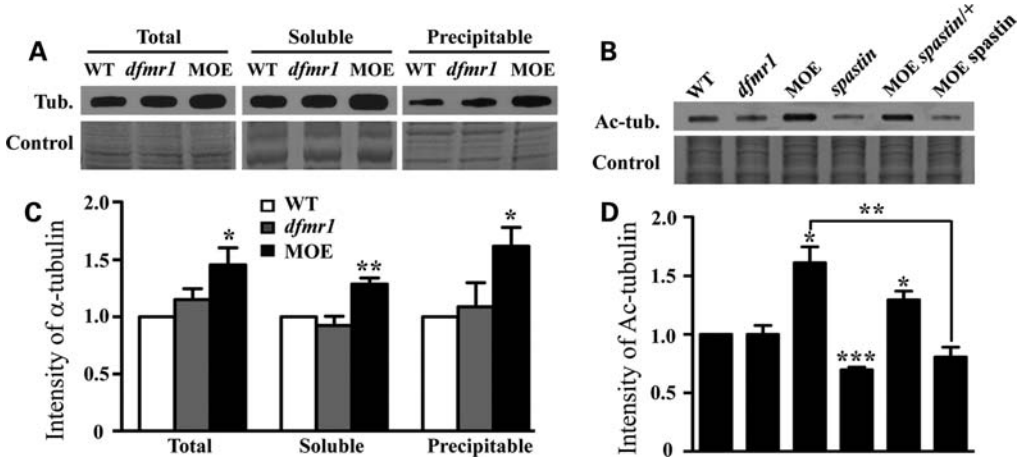

Figure 7. The amount of polymerized MTs is increased when *dfmr1* is over-expressed. (**A**) Expression levels of total, soluble and precipitable tubulins detected by anti-α-tubulin in three genotypes: wild-type (WT), $dfmr1^{50M}$ null mutants and *dfmr1* over-expression (MOE) in muscles (*C57-Gal4/UAS-dfmr1*). Equal loading (control) was demonstrated by a strip of gel with unknown proteins stained with Coomassie brilliant blue. (**B**) Expression levels of acetylated α-tubulins (Ac-tub.) detected by anti-acetylated α-tubulin in different genotypes. (**C** and **D**) Normalized intensities of α-tubulin [$n = 5$, (C)] and acetylated α-tubulin [$n = 4$, (D)] in different genotypes. $^{*}P < 0.05$, $^{**}P < 0.01$ and $^{***}P < 0.001$; error bars indicate SEM.

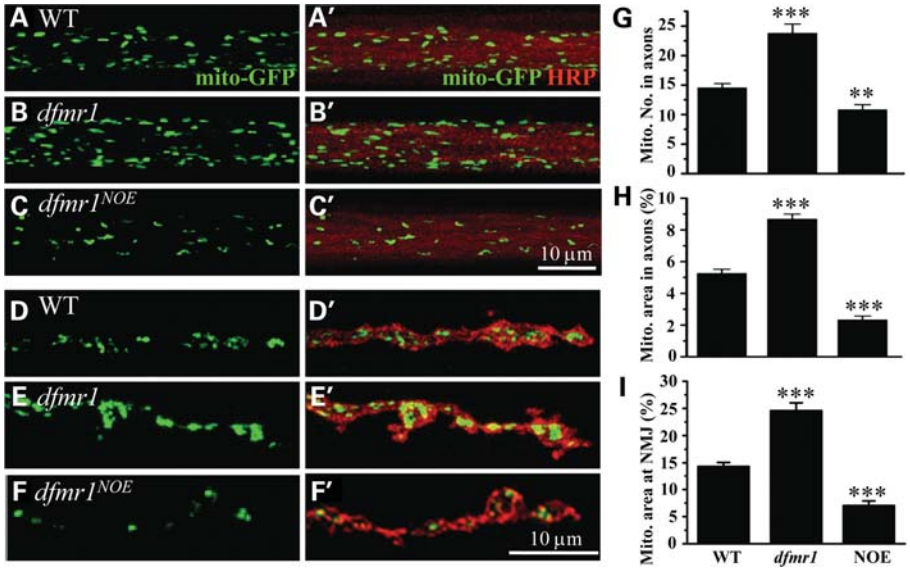

Figure 8. *dfmr1* negatively regulates the number of mitochondria in axons and NMJ synapses. Double labelling of axons (**A**–**C**) and NMJ synapses (**D**–**F**) with mito-GFP in green and anti-HRP in red recognizing neuronal membrane. Compared with the wild-type [(A) and (D)], increased number of mitochondria was observed in $dfmr1^{50M}$ mutants [(B) and (E)], and the opposite was observed when *dfmr1* was over-expressed in motor neurons driven by *D42-Gal4* [NOE; (C) and (F)]. Statistical results of the number (**G**) and area (**H**) of mitochondria in 100 μm^2 axons, and the area of mitochondria per 100 μm^2 NMJ4 terminals (**I**) in different genotypes. $^{**}P < 0.01$, $^{***}P < 0.001$; $n \geq 6$; error bars indicate SEM.

net velocity. To distinguish between the two possibilities, we quantified the speed of moving mitochondria. The velocity for both anterograde and retrograde transport in loss- and gain-of-function *dfmr1* mutants was comparable to that of wild-type (data not shown). These results show that *dfmr1* negatively regulates the flux of mitochondrial transport in axons.

To determine whether *dfmr1* controls additional transport parameters, we measured the length of time that mitochondria spent in forward runs (FRs), reverse runs (RRs) and stops. Although *dfmr1* mutants showed normal axonal transport of mitochondria in both directions (Fig. 9E), $dfmr1^{NOE}$ led to significantly decreased FR time (46.7 ± 2.16% for $dfmr1^{NOE}$ versus 54.16 ± 1.50% for wild-type in anterograde transport and 50.99 ± 1.29% for $dfmr1^{NOE}$ versus 59.07 ± 2.9% for wild-type in retrograde transport), but increased stop time (46.9 ± 1.62% for $dfmr1^{NOE}$ versus 39.27 ± 0.99% for wild-type in anterograde transport and 43.45 ± 1.17% for $dfmr1^{NOE}$ versus 35.09 ± 1.28% for wild-type in retrograde transport) (Fig. 9E). In summary, *dfmr1* mutants showed increased flux, whereas $dfmr^{NOE}$ animals exhibited reduced flux in both directions. In addition, $dfmr1^{NOE}$ animals

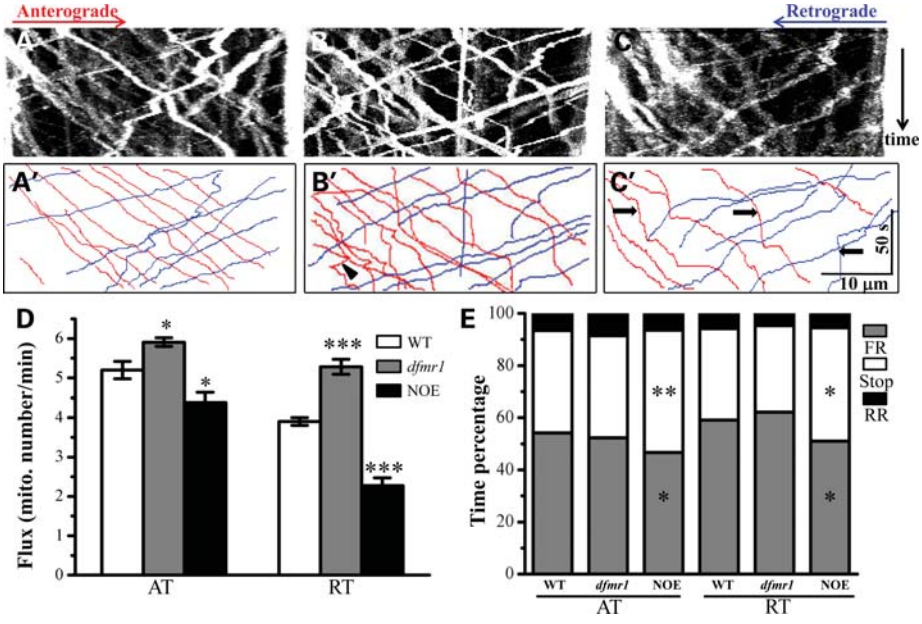

Figure 9. *dfmr1* affects bidirectional axonal transport of mitochondria. (**A**–**C**) Representative kymographs of mitochondrial transport in heterozygous control [*D42-Gal4 UAS-mito-GFP/+*, (A)], *dfmr1* mutants [*D42-Gal4 UAS-mito-GFP* $dfmr1^{50M}/dfmr1^{50M}$, (B)] and $dfmr1^{NOE}$ animals [*D42-Gal4 UAS-mito-GFP/UAS-dfmr1*, (C)]. Mitochondria moving in anterograde and retrograde directions appear as oblique lines. (**A′**–**C′**) Lines drawn by hand based on the images of (A–C), respectively, to better illustrate mitochondrial movements. Anterograde transport is shown in red and retrograde transport is shown in blue. Arrowheads in (B′) indicate reversals; horizontal arrows in (C′) denote stops. The horizontal scale bar represents 10 μm, and the vertical scale bar represents 50 s. Flux of mitochondrial transport (**D**) and the time of mitochondria stayed in FRs, RRs and stops (**E**) in different genotypes are quantitatively analysed and presented. AT, anterograde transport; RT, retrograde transport. $^{*}P < 0.05$, $^{**}P < 0.01$, $^{***}P < 0.001$; $n \geq 10$; error bars indicate SEM.

showed increased stop time. These findings demonstrate that *dfmr1* affects flux and processivity of mitochondrial transport in axons.

DISCUSSION

dfmr1 acts upstream of or in parallel with *spastin* in multiple processes

Previous studies identified several *dfmr1* interacting genes such as *futsch* (10), *cyfip* (31) and *ago1* (32). In the present study, we report *spastin* as a novel interactor of *dfmr1*. We identified robust genetic interactions between *dfmr1* and *spastin* in multiple contexts. First, *dfmr1* and *spastin* mutants have similar phenotypes such as overgrown NMJ synapses (Fig. 2), faster roll-over locomotion (Fig. 3), broken MT fibres (Fig. 4) and increased level of Futsch at synaptic terminals (Fig. 5), suggesting that the two genes act similarly in different processes. Secondly, the prominent *dfmr1* over-expression phenotypes can be effectively rescued by heterozygous (Figs 1 and 3) and homozygous *spastin* null mutations (Figs 2–5), i.e. *spastin* is required for the $dfmr1^{OE}$ toxicity. Conversely, *spastin* null phenotypes can be rescued by *dfmr1* over-expression (Figs 2–5), suggesting a novel strategy to interrupt the spastin-related pathogenesis. It would be informative to also examine the interaction in the reciprocal configuration, i.e. over-expression of *spastin* in a *dfmr1* null background. Unfortunately, as we reported earlier (22), the dominance of *spastin* over-expression precluded the interaction assay. The rescue of *dfmr1* over-expression phenotypes by *spastin* mutants (Figs 1–5) and the reciprocal rescuing effect (Figs 2–5) indicate that *dfmr1* acts upstream of or in parallel with *spastin*. As spastin is sufficient to directly sever MTs (16,17,22), it is unlikely that spastin acts through dFMRP. Western analysis showed that the level of spastin was increased significantly when *dfmr1* was over-expressed, whereas *spastin* had no effect on the expression of *dfmr1* (Fig. 6), in support of the epistatic interaction of *dfmr1* acting upstream of *spastin*. It is worth pointing out that although the requirement of *spastin* for the $dfmr1^{OE}$ toxicity is robust and consistent in the six systems we examined (Figs 1–5 and 7), the interaction does not apply to the mitochondria transport (Supplementary Material, Fig. S2), indicating that the interaction is context-dependent. Thirdly, the *dfmr1 spastin* double null mutants showed stronger NMJ morphological defects than the single mutants (Fig. 2), supporting the point that the action of *dfmr1* is parallel with that of *spastin*. Consistent with the parallel function between *dfmr1* and *spastin*, we found no association between dFMRP and spastin by co-immunoprecipitation assay (data not shown). Taken together, the epistatic and biochemical analyses show that *dfmr1* acts upstream of or in parallel with *spastin*.

dfmr1 regulates MT network formation

This study provides the first experimental evidence of an abnormal MT network when *dfmr1* expression is altered in *Drosophila*. There were more perinuclear MTs, but reduced MTs with tangles and short MT fibres in areas distal to the nuclei of *dfmr1* mutant muscle cells. On the contrary, *dfmr1* over-expression resulted in thick parallel MT bundles with elevated expressions of α-tubulin and acetylated MTs

(Figs 4 and 7). The mechanism by which dFMRP regulates the formation of the MT network is currently unknown. However, there are several possibilities. First, FMRP associates with MTs as detected by a fractionation assay (8,9), and the absence of FMRP might thus affect MTs directly or indirectly. Secondly, FMRP has been shown to interact directly with motor proteins such as KIF3C (8) and KLC (13). It is well known that motors such as kinesin-like protein at 61F (KLP61F) and dynein can bundle and slide MTs (33,34). Thus, dFMRP could regulate MTs by its interacting motors. Thirdly, FMRP represses the translation of MAP1B and is required for the accelerated decline of MAP1B during synaptogenesis in the neonatal mouse brain (7). The thick parallel MT bundles and increased α-tubulin expression in *dfmr1*^{MOE} animals are similar to those in *futsch* mutants (24). Furthermore, *dfmr1* interacts with *futsch* but not with *spastin* in regulating axonal transport (Supplementary Material, Fig. S2). However, Futsch is expressed only in the nervous system (35), whereas dFMRP is widely expressed in multiple tissues, including muscles, indicating that there might be targets other than Futsch by which dFMRP regulates MTs in non-neuronal cells. Last, but not the least, given that the epistatic analysis revealed parallel functions between *dfmr1* and *spastin* in multiple processes (Figs 1–5 and 7), it is conceivable that *dfmr1* might regulate MTs in a manner similar to that of spastin or via spastin. In summary, *dfmr1* might regulate MTs through distinct mechanisms involving different partners in different cellular contexts. It would be of interest to unravel the mechanism by which dFMRP regulates MTs.

dfmr1 regulates the number and transport of mitochondria

One surprising finding is that *dfmr1* negatively regulates the number of mitochondria (Fig. 8). There are many reports of reduced numbers of mitochondria in axons or synaptic terminals when a gene is disrupted, but the opposite was rarely documented (36). Mitochondrial transport to synapse is tightly regulated to provide sufficient energy for synaptic transmission (37,38). Decreased synaptic transmission has been reported to be associated with reduced numbers of functional mitochondria (30,36,39). Consistently, the increased number of mitochondria (Fig. 8) is positively correlated with elevated neurotransmission at the NMJ synapses in *dfmr1* mutants (10). The mechanism by which *dfmr1* negatively regulates the number of mitochondria remains to be elucidated.

We have demonstrated for the first time that *dfmr1* affects axonal transport of mitochondria. The flux of both anterograde and retrograde transport is increased in *dfmr1* mutants, but reduced in *dfmr1*^{NOE} animals (Fig. 9). Additionally, in *dfmr*^{NOE} animals, there was reduced time in FRs but increased stop time in the mitochondrial transport of both directions, indicative of more 'stop signs' for axonal transport. The altered flux of mitochondrial transport in both loss- and gain-of-function *dfmr1* mutants is positively correlated with the altered numbers of mitochondria (Figs 8 and 9). It has been shown that FMRP co-localizes with mRNA in granules (40,41). In RNA granule transport, FMRP associates with motor proteins such as KLC, kinesin heavy chain, KIF3C and dynein (42). Loss of dFMRP causes increased bidirectional and oscillatory movement of mRNA granules (42). Fluorescence recovery after photobleaching (FRAP) analysis showed that the fluorescence recovery rate of mRNA granules is reduced in *dfmr1* mutants (42). Thus, FMRP acts as a processivity factor for mRNA transport and a molecular adaptor between RNA granules and motor proteins (8,42).

The transport of mitochondria depends on MTs (26) and so does the transport of FMRP-positive mRNA granules (40,41). MT-severing spastin regulates mitochondrial localization and transport; expressing mutant spastin in neurons results in abnormal perinuclear clusters of mitochondria (43). More recently, a reduction in the anterograde flux of mitochondrial transport was reported in cultured neurons from *spastin* mutant mice (44). We showed that the flux of both anterograde and retrograde mitochondrial transport was decreased in *Drosophila spastin* mutants, similar to that observed in *dfmr1*^{NOE} animals (Fig. 9 and Supplementary Material, Fig. S2). Consequently, *spastin* mutants did not rescue the transport defects in *dfmr1*^{NOE} animals (Supplementary Material, Fig. S2), although the rescue effect has been observed readily in multiple other contexts (Figs 1–5 and 7), indicating that the interactions between the two genes may work differently in different systems (axonal transport versus other processes) or that axonal transport requires special machinery not related to the *dfmr1–spastin* interaction. In contrast, *futsch* mutants showed reduced flux of mitochondrial transport, similar to that observed in *dfmr*^{NOE} animals, but opposite to that of *dfmr1* mutants (Supplementary Material, Fig. S2). Interestingly, *futsch* mutants rescued the increased flux of mitochondrial transport in *dfmr1* mutants (Supplementary Material, Fig. S2), which supports the previous finding that *dfmr1* negatively regulates *futsch* (10,11,24). We therefore favour the hypothesis that *dfmr1* might regulate mitochondrial transport by affecting MTs mainly through Futsch, although *dfmr1* and *spastin* interact in other cellular contexts such as synapse growth, locomotive control and MT network formation.

MATERIALS AND METHODS

Drosophila stocks and genetics

Drosophila w^{1118} flies were used as the wild-type control. All flies were cultured in standard cornmeal medium at 25°C. The *Drosophila* stocks used in this study include the eye-specific *GMR-Gal4*, the muscle-specific *C57-Gal4* and the pan-neuronal *elav-Gal4*. *dfmr1*-related stocks *EP3517*, *UAS-dfmr1* and *dfmr1*^{50M} null allele with a large intragenic deletion were described previously (10). Transgenic flies carrying a genomic rescue construct P[w^+: *dfmr1*] on the second chromosome were from Siomi and co-workers (45). *spastin* hypomorph *spastin*$^{17\text{-}7}$ and null allele *spastin*$^{5.75}$, which has coding sequences completely deleted, were from Sherwood *et al.* (16). Multiple *UAS-spastin* and *spastin* RNAi lines were from Sherwood *et al.* (16) and Broadie and co-workers (17). *sev-dfmr1* was from Zarnescu *et al.* (20). *D42-Gal4 UAS-mito-GFP/TM6B* was from Saxton and co-workers (27). Chromosomal recombinants used for genetic interaction assay were made following conventional genetic techniques.

Larval roll-over assay

The larval roll-over assay was performed essentially as described previously (46). Before the assay, larval cultures and agar plates were kept at room temperature for 2 h to acclimatize. For each assay, an individual animal was placed onto a 1% agar plate and allowed to move freely for ~2 min. A test animal that moved in a straight line was rolled over by a soft brush to a completely inverted position, as indicated by the ventral midline facing up. The length of time that the animal took to totally right itself was recorded. Three consecutive assays were performed for each animal and then averaged. The data were analysed by two-tailed Student's *t*-test.

Immunostaining, confocal microscopy and quantitative analysis

Dissection and antibody staining of wandering third instar larvae were as described (10,22). The primary antibodies used include anti-α-tubulin (1:1000; mAb B-5-1-2 from Sigma, St Louis, Mossouri), anti-CSP [1:500; 6D6 from the Developmental Studies Hybridoma Bank (DSHB) at the University of Iowa], anti-Futsch (1:50; 22C10 from DSHB) and FITC and Texas red-conjugated anti-HRP (used at 1:100; Jackson ImmunoResearch, West Grove, Pennsylvania). The primary antibodies were detected using Alexa 488 or Alexa 568 conjugated goat anti-mouse IgG (1:1500; Invitrogen, Carlsbad, California). Nuclei were labelled by staining with 1.25 μg/ml propidium iodide (PI) at room temperature for 30 min. Images were collected with a Leica SP5 confocal microscope and processed using Adobe Photoshop.

NMJ phenotypes were quantified essentially according to published protocols (10,22). All images analysed were three-dimensional (3D) projections from complete Z-stacks through the entire NMJ4 of abdominal segment A3. A synaptic branch was defined on the basis of anti-HRP staining; the elaboration originating directly from the nerve entry point was defined as primary branches, and each higher order branch was counted only when two or more boutons could be discerned in the subsequent branch. Individual boutons were defined according to the discrete staining signal of anti-CSP (a synaptic vesicle marker). Bouton size was calculated by dividing the synaptic area by the number of boutons. The synaptic area was determined by measuring the area of anti-CSP staining of the whole synaptic terminal with ImageJ. At least 19 animals were analysed for each genotype.

The intensity of tubulin staining in different genotypes was quantified, as described previously (22). Specifically, muscle 2 in abdominal segment A4 was chosen for analysis because it has fewer tracheal branches to obscure the observation of MTs (22). For quantification of MTs detected by anti-α-tubulin staining in muscles, all images analysed were 3D projections of serial stacks through the muscle cell. The perinuclear area was defined as the coverage that spans a 5 μm diameter circular ring next to nuclei. The middle of the 10×10 μm square marked in Figure 4A was defined as the central area among nuclei. Anti-α-tubulin staining signals in the perinuclear or central area were calculated using ImageJ. The software reports the grey value of the selected area. MT breakpoints in the central areas (20×20 μm^2) of muscle cells stained with anti-α-tubulin were counted and compared. Breakpoints were defined as the ends of an MT fibre. If both ends of an MT fibre were present in the analysed area, it was recorded as one breakpoint. Six to eight larvae of each genotype were analysed per experiment, and three repeats were conducted for quantification analysis.

For quantification of the fluorescence intensity of Futsch, all images of the whole NMJ4 elaborations of different genotypes were taken at identical settings without over-exposure. The intensity of Futsch in Figure 5 was presented as grey values normalized to the Futsch-positive area automatically calculated using ImageJ.

Protein preparation and western analysis

Third instar larvae were dissected in phosphate-buffered saline (PBS). All internal organs were removed, and the remaining fillet containing largely muscles was homogenized on ice in lysis buffer [100 mM KCl, 2 mM $MgCl_2$, 50 mM Tris (pH 7.5), 2 mM ethylene glycol tetraacetic acid, 2% (v/v) glycerol, 0.125% (v/v) Triton X-100, 100 nM paclitaxel (Invitrogen), 1% (v/v) dimethyl sulphoxide and 1% Protease Inhibitor Cocktail (Calbiochem, Darmstadt, Germany)]. After centrifugation at room temperature for 3 min at 500*g*, the supernatant was recovered and centrifuged at 4°C for 1 h at 100 000*g*. The supernatant was recovered and used to determine the amount of soluble tubulin. The pellet was suspended in lysis buffer to assess the precipitated, presumably polymerized, tubulin. Protein concentration was determined by the Bradford assay (Bio-Rad, Foster, California). Equal amounts of protein from different genotypes were mixed with 2× Laemmli buffer, resolved by sodium dodecyl sulphate–polyacrylamide gel electrophoresis and transferred to polyvinylidene fluoride membranes. The blots were first probed with mouse monoclonal antibodies against α-tubulin (Sigma, 1:30 000), acetylated-α-tubulin (Sigma, 1:30 000), actin (mAb1501 from Chemicon, Rosemont, Illinois; 1:50 000), dFMRP (6A15 from Sigma, 1:2000) or guinea pig polyclonal antibody against spastin (a gift from Sherwood, 1:1000) followed by incubation with HRP-conjugated corresponding secondary antibodies (Sigma, 1:10 000). The processed membrane was developed with the chemiluminescent HRP substrate (Millipore, Billerica, Massachusetts) to detect target proteins. To quantify the expression levels of α-tubulin, acetylated α-tubulin and spastin in different genotypes, the positive signals from multiple repeats were calculated using ImageJ software and normalized against that of the wild-type.

Scanning electron microscopy (SEM) of the eye

SEM was adapted from a published protocol (47). Specifically, adult flies were fixed in 2.5% (v/v) glutaraldehyde in 0.1 M PBS (pH 7.2) for 2 h, followed by washing in PBS for 30 min. The fixed heads were removed, dehydrated in a graded ethanol series, followed by drying and sputter coating and finally examined with a HITACHIS-3000N SEM instrument.

Live imaging, tracking and analysis of GFP-tagged mitochondrial transport in axons

The analysis of mitochondrial transport was performed essentially as described (28). Wandering third instar larvae carrying the mito-GFP marker driven by the motor neuron-specific *D42-Gal4* were dissected quickly in HL6 solution and then imaged directly at room temperature with a Leica SP5 confocal microscope under a 40× water immersion objective. To allow tracking of long-range mitochondrial transport, a 40 μm region of the segmental nerve was photobleached with 488 nm light at full intensity before image collection. Image collections were made every 1 s on a single plane for 5 min and completed within 15 min after dissection. The movements of mitochondria into or through the photobleached region were tracked and analysed by ImageJ (28) and plugin MTrackJ (E. Meijering, Biomedical Imaging Group of Rotterdam, The Netherlands; http://www.imagescience.org/meijering/software/mtrackj/ last accessed on October 13). Motile mitochondria were tracked as long as each remained visible in consecutive frames for no less than 60 s. The *x-y-t* tracking coordinates of mitochondrial movements calculated by MTrackJ were exported to modified Excel-based software (28,29) for automated analysis.

For quantitative analysis, mitochondrial transport was described in a three-state system consisting of FRs, RRs and stops adapted from Russo *et al*. (29). The start of a run was defined as a minimal speed of 0.151 μm/s and the end of a run by a velocity no less than 0.12 μm/s. A stop was defined in the MTrackJ program as no motility, moving at <0.12 μm/s following a run or <0.151 μm/s before a run starts (28,29). The following motility parameters were analysed: net velocity of anterograde and retrograde transport and the percentage of time spent in runs and stops. Flux was calculated by counting the number of mitochondria that moved past the anterior (anterograde flux) and posterior (retrograde flux) boundaries of the photobleached area per minute for 5 min.

SUPPLEMENTARY MATERIAL

Supplementary Material is available at *HMG* online.

ACKNOWLEGEMENTS

We thank N. Sherwood and K. Broadie for *spastin* mutants and transgenic *UAS-spastin* and *spastin* RNAi flies, M. Saxton for *D42-Gal4 UAS-mito-GFP/TM6B*, D. Zarnescu for *sev-dfmr1*, H. Siomi for *dfmr1* genomic rescue P[w^+: *dfmr1*] flies, Dan Wang for assistance in initial genetic screens for *dfmr1* interactors and N. Sherwood for spastin antibodies. We are grateful to the Bloomington Stock Centre for fly stocks and the Developmental Studies Hybridoma Bank, University of Iowa for antibodies. Dr Q. Hu at the Institute of Neuroscience, Shanghai Institutes for Biological Sciences, assisted in the analysis of axonal transport. We thank Edouard Khandjian, Ming Guo, Chonglin Yang, Xun Huang and Lily Jan for helpful discussions on the manuscript.

Conflict of Interest statement. None declared.

FUNDING

This work was supported by grants from the National Science Foundation of China (NSFC; 30930033) and the Ministry of Science and Technology of China (2007CB947200) to Y.Q.Z. and from NSFC (30800324) to A.Y.

REFERENCES

1. Bagni, C. and Greenough, W.T. (2005) From mRNP trafficking to spine dysmorphogenesis: the roots of fragile X syndrome. *Nat. Rev. Neurosci.*, **6**, 376–387.
2. Zhang, Y.Q. and Broadie, K. (2005) Fathoming fragile X in fruit flies. *Trends Genet.*, **21**, 37–45.
3. Penagarikano, O., Mulle, J.G. and Warren, S.T. (2007) The pathophysiology of fragile X syndrome. *Annu. Rev. Genomics Hum. Genet.*, **8**, 109–129.
4. Brown, V., Jin, P., Ceman, S., Darnell, J.C., O'Donnell, W.T., Tenenbaum, S.A., Jin, X., Feng, Y., Wilkinson, K.D., Keene, J.D. *et al.* (2001) Microarray identification of FMRP-associated brain mRNAs and altered mRNA translational profiles in fragile X syndrome. *Cell*, **107**, 477–487.
5. Darnell, J.C., Jensen, K.B., Jin, P., Brown, V., Warren, S.T. and Darnell, R.B. (2001) Fragile X mental retardation protein targets G quartet mRNAs important for neuronal function. *Cell*, **107**, 489–499.
6. Zalfa, F., Giorgi, M., Primerano, B., Moro, A., Di Penta, A., Reis, S., Oostra, B. and Bagni, C. (2003) The fragile X syndrome protein FMRP associates with BC1 RNA and regulates the translation of specific mRNAs at synapses. *Cell*, **112**, 317–327.
7. Lu, R., Wang, H., Liang, Z., Ku, L., O'Donnell, W.T., Li, W., Warren, S.T. and Feng, Y. (2004) The fragile X protein controls microtubule-associated protein 1B translation and microtubule stability in brain neuron development. *Proc. Natl Acad. Sci. USA*, **101**, 15201–15206.
8. Davidovic, L., Jaglin, X.H., Lepagnol-Bestel, A.M., Tremblay, S., Simonneau, M., Bardoni, B. and Khandjian, E.W. (2007) The fragile X mental retardation protein is a molecular adaptor between the neurospecific KIF3C kinesin and dendritic RNA granules. *Hum. Mol. Genet.*, **16**, 3047–3058.
9. Wang, H., Dictenberg, J.B., Ku, L., Li, W., Bassell, G.J. and Feng, Y. (2008) Dynamic association of the fragile X mental retardation protein as a messenger ribonucleoprotein between microtubules and polyribosomes. *Mol. Biol. Cell*, **19**, 105–114.
10. Zhang, Y.Q., Bailey, A.M., Matthies, H.J., Renden, R.B., Smith, M.A., Speese, S.D., Rubin, G.M. and Broadie, K. (2001) *Drosophila* fragile X-related gene regulates the MAP1B homolog Futsch to control synaptic structure and function. *Cell*, **107**, 591–603.
11. Chang, S., Bray, S.M., Li, Z., Zarnescu, D.C., He, C., Jin, P. and Warren, S.T. (2008) Identification of small molecules rescuing fragile X syndrome phenotypes in *Drosophila*. *Nat. Chem. Biol.*, **4**, 256–263.
12. Kanai, Y., Dohmae, N. and Hirokawa, N. (2004) Kinesin transports RNA: isolation and characterization of an RNA-transporting granule. *Neuron*, **43**, 513–525.
13. Dictenberg, J.B., Swanger, S.A., Antar, L.N., Singer, R.H. and Bassell, G.J. (2008) A direct role for FMRP in activity-dependent dendritic mRNA transport links filopodial-spine morphogenesis to fragile X syndrome. *Dev. Cell*, **14**, 926–939.
14. Ling, S.C., Fahrner, P.S., Greenough, W.T. and Gelfand, V.I. (2004) Transport of *Drosophila* fragile X mental retardation protein-containing ribonucleoprotein granules by kinesin-1 and cytoplasmic dynein. *Proc. Natl Acad. Sci. USA*, **101**, 17428–17433.
15. Hazan, J., Fonknechten, N., Mavel, D., Paternotte, C., Samson, D., Artiguenave, F., Davoine, C.S., Cruaud, C., Durr, A., Wincker, P. *et al.* (1999) Spastin, a new AAA protein, is altered in the most frequent form of autosomal dominant spastic paraplegia. *Nat. Genet.*, **23**, 296–303.
16. Sherwood, N.T., Sun, Q., Xue, M., Zhang, B. and Zinn, K. (2004) *Drosophila* spastin regulates synaptic microtubule networks and is required for normal motor function. *PLoS Biol.*, **2**, e429.

17. Trotta, N., Orso, G., Rossetto, M.G., Daga, A. and Broadie, K. (2004) The hereditary spastic paraplegia gene, spastin, regulates microtubule stability to modulate synaptic structure and function. *Curr. Biol.*, **14**, 1135–1147.
18. Roll-Mecak, A. and Vale, R.D. (2005) The *Drosophila* homologue of the hereditary spastic paraplegia protein, spastin, severs and disassembles microtubules. *Curr. Biol.*, **15**, 650–655.
19. Brand, A.H. and Perrimon, N. (1993) Targeted gene expression as a means of altering cell fates and generating dominant phenotypes. *Development*, **118**, 401–415.
20. Zarnescu, D.C., Jin, P., Betschinger, J., Nakamoto, M., Wang, Y., Dockendorff, T.C., Feng, Y., Jongens, T.A., Sisson, J.C., Knoblich, J.A. *et al.* (2005) Fragile X protein functions with lgl and the par complex in flies and mice. *Dev. Cell*, **8**, 43–52.
21. Gatto, C.L. and Broadie, K. (2008) Temporal requirements of the fragile X mental retardation protein in the regulation of synaptic structure. *Development*, **135**, 2637–2648.
22. Jin, S., Pan, L., Liu, Z., Wang, Q., Xu, Z. and Zhang, Y.Q. (2009) *Drosophila* tubulin-specific chaperone E functions at neuromuscular synapses and is required for microtubule network formation. *Development*, **136**, 1571–1581.
23. Errico, A., Ballabio, A. and Rugarli, E.I. (2002) Spastin, the protein mutated in autosomal dominant hereditary spastic paraplegia, is involved in microtubule dynamics. *Hum. Mol. Genet.*, **11**, 153–163.
24. Bettencourt da Cruz, A., Schwarzel, M., Schulze, S., Niyyati, M., Heisenberg, M. and Kretzschmar, D. (2005) Disruption of the MAP1B-related protein FUTSCH leads to changes in the neuronal cytoskeleton, axonal transport defects, and progressive neurodegeneration in *Drosophila*. *Mol. Biol. Cell*, **16**, 2433–2442.
25. Hammond, J.W., Cai, D. and Verhey, K.J. (2008) Tubulin modifications and their cellular functions. *Curr. Opin. Cell Biol.*, **20**, 71–76.
26. Hollenbeck, P.J. and Saxton, W.M. (2005) The axonal transport of mitochondria. *J. Cell Sci.*, **118**, 5411–5419.
27. Pilling, A.D., Horiuchi, D., Lively, C.M. and Saxton, W.M. (2006) Kinesin-1 and dynein are the primary motors for fast transport of mitochondria in *Drosophila* motor axons. *Mol. Biol. Cell*, **17**, 2057–2068.
28. Louie, K., Russo, G.J., Salkoff, D.B., Wellington, A. and Zinsmaier, K.E. (2008) Effects of imaging conditions on mitochondrial transport and length in larval motor axons of *Drosophila*. *Comp. Biochem. Physiol. A Mol. Integr. Physiol.*, **151**, 159–172.
29. Russo, G.J., Louie, K., Wellington, A., Macleod, G.T., Hu, F., Panchumarthi, S. and Zinsmaier, K.E. (2009) *Drosophila* Miro is required for both anterograde and retrograde axonal mitochondrial transport. *J. Neurosci.*, **29**, 5443–5455.
30. Chee, F.C., Mudher, A., Cuttle, M.F., Newman, T.A., MacKay, D., Lovestone, S. and Shepherd, D. (2005) Over-expression of tau results in defective synaptic transmission in *Drosophila* neuromuscular junctions. *Neurobiol. Dis.*, **20**, 918–928.
31. Schenck, A., Bardoni, B., Langmann, C., Harden, N., Mandel, J.L. and Giangrande, A. (2003) CYFIP/Sra-1 controls neuronal connectivity in *Drosophila* and links the Rac1 GTPase pathway to the fragile X protein. *Neuron*, **38**, 887–898.
32. Jin, P., Zarnescu, D.C., Ceman, S., Nakamoto, M., Mowrey, J., Jongens, T.A., Nelson, D.L., Moses, K. and Warren, S.T. (2004) Biochemical and genetic interaction between the fragile X mental retardation protein and the microRNA pathway. *Nat. Neurosci.*, **7**, 113–117.
33. van den Wildenberg, S.M., Tao, L., Kapitein, L.C., Schmidt, C.F., Scholey, J.M. and Peterman, E.J. (2008) The homotetrameric kinesin-5 KLP61F preferentially crosslinks microtubules into antiparallel orientations. *Curr. Biol.*, **18**, 1860–1864.
34. Ferenz, N.P., Paul, R., Fagerstrom, C., Mogilner, A. and Wadsworth, P. (2009) Dynein antagonizes eg5 by crosslinking and sliding antiparallel microtubules. *Curr. Biol.*, **19**, 1833–1838.
35. Hummel, T., Krukkert, K., Roos, J., Davis, G. and Klambt, C. (2000) *Drosophila* Futsch/22C10 is a MAP1B-like protein required for dendritic and axonal development. *Neuron*, **26**, 357–370.
36. Goldstein, A.Y., Wang, X. and Schwarz, T.L. (2008) Axonal transport and the delivery of pre-synaptic components. *Curr. Opin. Neurobiol.*, **18**, 495–503.
37. Ly, C.V. and Verstreken, P. (2006) Mitochondria at the synapse. *Neuroscientist*, **12**, 291–299.
38. Wang, X. and Schwarz, T.L. (2009) Imaging axonal transport of mitochondria. *Methods Enzymol.*, **457**, 319–333.
39. Verstreken, P., Ly, C.V., Venken, K.J., Koh, T.W., Zhou, Y. and Bellen, H.J. (2005) Synaptic mitochondria are critical for mobilization of reserve pool vesicles at *Drosophila* neuromuscular junctions. *Neuron*, **47**, 365–378.
40. De Diego Otero, Y., Severijnen, L.A., van Cappellen, G., Schrier, M., Oostra, B. and Willemsen, R. (2002) Transport of fragile X mental retardation protein via granules in neurites of PC12 cells. *Mol. Cell. Biol.*, **22**, 8332–8341.
41. Antar, L.N., Dictenberg, J.B., Plociniak, M., Afroz, R. and Bassell, G.J. (2005) Localization of FMRP-associated mRNA granules and requirement of microtubules for activity-dependent trafficking in hippocampal neurons. *Genes Brain Behav.*, **4**, 350–359.
42. Estes, P.S., O'Shea, M., Clasen, S. and Zarnescu, D.C. (2008) Fragile X protein controls the efficacy of mRNA transport in *Drosophila* neurons. *Mol. Cell. Neurosci.*, **39**, 170–179.
43. McDermott, C.J., Grierson, A.J., Wood, J.D., Bingley, M., Wharton, S.B., Bushby, K.M. and Shaw, P.J. (2003) Hereditary spastic paraparesis: disrupted intracellular transport associated with spastin mutation. *Ann. Neurol.*, **54**, 748–759.
44. Kasher, P.R., De Vos, K.J., Wharton, S.B., Manser, C., Bennett, E.J., Bingley, M., Wood, J.D., Milner, R., McDermott, C.J., Miller, C.C. *et al.* (2009) Direct evidence for axonal transport defects in a novel mouse model of mutant spastin-induced hereditary spastic paraplegia (HSP) and human HSP patients. *J. Neurochem.*, **110**, 34–44.
45. Inoue, S., Shimoda, M., Nishinokubi, I., Siomi, M.C., Okamura, M., Nakamura, A., Kobayashi, S., Ishida, N. and Siomi, H. (2002) A role for the *Drosophila* fragile X-related gene in circadian output. *Curr. Biol.*, **12**, 1331–1335.
46. Pan, L., Woodruff, E. III, Liang, P. and Broadie, K. (2008) Mechanistic relationships between *Drosophila* fragile X mental retardation protein and metabotropic glutamate receptor A signaling. *Mol. Cell. Neurosci.*, **37**, 747–760.
47. Kimmel, B.E., Heberlein, U. and Rubin, G.M. (1990) The homeo domain protein rough is expressed in a subset of cells in the developing *Drosophila* eye where it can specify photoreceptor cell subtype. *Genes Dev.*, **4**, 712–727.